Group-theoretical analysis of two-dimensional hexagonal materials

Group theoretical analysis of two-dimensional hexagonal materials

Susumu Minami[1], Itaru Sugita[1], Ryosuke Tomita[1], Hiroyuki Oshima[1] and Mineo Saito[2]

[1]*Graduation school of mathematics and physics, Kanazawa Univ., Kakuma, Kanazawa, 920-1192, Japan*

[2]*Division of mathematical and physical science, Kanazawa Univ., Kakuma, Kanazawa, 920-1192, Japan*

Two-dimensional hexagonal materials such as graphene and silicene have high symmetric crystal structures and Dirac-cones at the K point which induce novel electronic properties appear. In this report, we calculate their electronic structures by using the density functional theory and analyze their band structures based on the group theory. Dirac cones frequently appear when the symmetry at the K point is high so that two-dimensional irreducible representations are included. We discuss the relation between symmetry and appearance of the Dirac cone.

1. Introduction

After the discovery of monolayer graphene, electronic structures of graphene have been extensively studied.[1] Carbon atoms form honeycomb structure and novel electronic structure of graphene is characterized by the Dirac cone, which is expected to induce useful electronic properties.[2–7] Because of its electronic characteristics, graphene is expected to be applied to nanoscale applications.[8–10] As well as graphene, silicene forms a hexagonal structure. The neighboring silicon atoms are buckled unlike graphene and thus the symmetry is lowered. In spite of this symmetry difference, the Dirac cone also appears at the K point in silicene.[11–14]

Furthermore, the two-dimensional hexagonal materials such as germanene and stanene have been synthesized.[15,16] Moreover V-element forms two-dimensional hexagonal sheet; phosphorene has been recently achieved.[17] Bi also forms ultrathin films having the hexagonal structures.[18] Therefore, understanding of electronic structures of these two-dimensional hexagonal materials attracts scientific interests. In particular, it is important to clarify which hexagonal materials induce Dirac cones. It should be noticed that high space symmetry including two-dimensional irreducible representations at the K point induces the Dirac cones since two bands are degenerated at the Dirac point. It is possible that other mechanisms induce Dirac cones beside the high space symmetry induced mechanism. Accidental degeneracies might induce Dirac cones[19,20]

and the Dirac cones can be induced in time-reversal systems affected by spin-orbit interaction.[21, 22] However, the above-mentioned high space symmetry induced Dirac cones are expected to be common for the two-dimensional hexagonal materials such as graphene and silecene. We therefore focus on this mechanism in this paper.

From the view point of the group theory, the two-dimensional hexagonal sheets form hexagonal or trigonal lattices, then the group theoretical analysis of these lattices is expected to give insight into the appearance of Dirac cones.[23, 24]

In this paper, we study monolayer and bilayer of graphene and silicene. We perform first-principles band structure calculation and examine the appearance of the Dirac cone. The calculation results are analyzed based on the group theory and we discuss the relation between the appearance of the Dirac cone and space symmetry.

2. Method

The symmetry operation $\hat{R}$ is given by

$$\hat{R} = \{\Theta|\tau\} \tag{1}$$

where Θ and τ represent rotation and translation, respectively.[25, 26] We consider the Bloch wavefunction, $\psi_i^{\boldsymbol{k}}(r)$, where $\boldsymbol{k}$ is the wavevector in the first Brillouin zone and i is the band index, which is in ascending order of the energy. When $\hat{R}$ operates the Bloch wave function, we obtain

$$\hat{R}\psi_i^{\boldsymbol{k}}(r) = \psi_i^{\boldsymbol{k}}(\Theta^{-1}r - \Theta^{-1}\tau) \tag{2}$$

The projection operator is introduced here,

$$\hat{P}_k^l = \frac{1}{h}\sum_{\hat{R}}\chi_k^l(\hat{R})\hat{R} \tag{3}$$

where h is the order of the k group and $\chi_k^l(\hat{R})$ is the character in the irreducible representation. The summation in eq.(3) runs over the symmetry operations which in the k group. By evaluationg the following expression, we can identify the irreducible representations of the wavefunctions of n-th degeneracy.

$$Q = \sum_i^n \int dr \psi_i^{\boldsymbol{k}}(r)^* \hat{P}_k^l \psi_i^{\boldsymbol{k}}(r) \tag{4}$$

When $Q = 1, (Q = 0)$, the wavefunctions (do not) belong to the l-th irreducible representation. We here introduce the irreducible ray representation[27]

$$\acute{\chi}_k^l = \exp(i\boldsymbol{k}\boldsymbol{\tau})\chi_k^l \tag{5}$$

The characters of the irreducible ray representation in most of cases correspond to those of point groups of Mulliken notation, which is used in analysis of molecules. In particular, the characters in all the systems in the present study can be denoted by using Mulliken notations. Therefore, we use the ray representation in this study and we simply refer to it as "representation" hereafter.

We implemented the above algorithm in first-principles calculation code PHASE/0.[28] Therefore the identification of the representations is carried out by using computers.

We carry out density-functional band-structure calculations to obtain the Bloch wavefunctions, $\psi_i^{\boldsymbol{k}}(r)$. We use the exchange-correlation functional of the generalized gradient approximation (GGA)[29] for the silicene. The local density approximation (LDA)[30] is used for graphene since it is better than the GGA in the case that the Van der Waals interaction is active.[31] We use slab models for simulating two-dimensional periodic systems. The ultra-soft[32] and norm-conserving[33] pseudo potentials are used for carbon and silicon atoms, respectively. The 24×24 and 16×16 k sampling points are used in the Brillouin zone integrations.
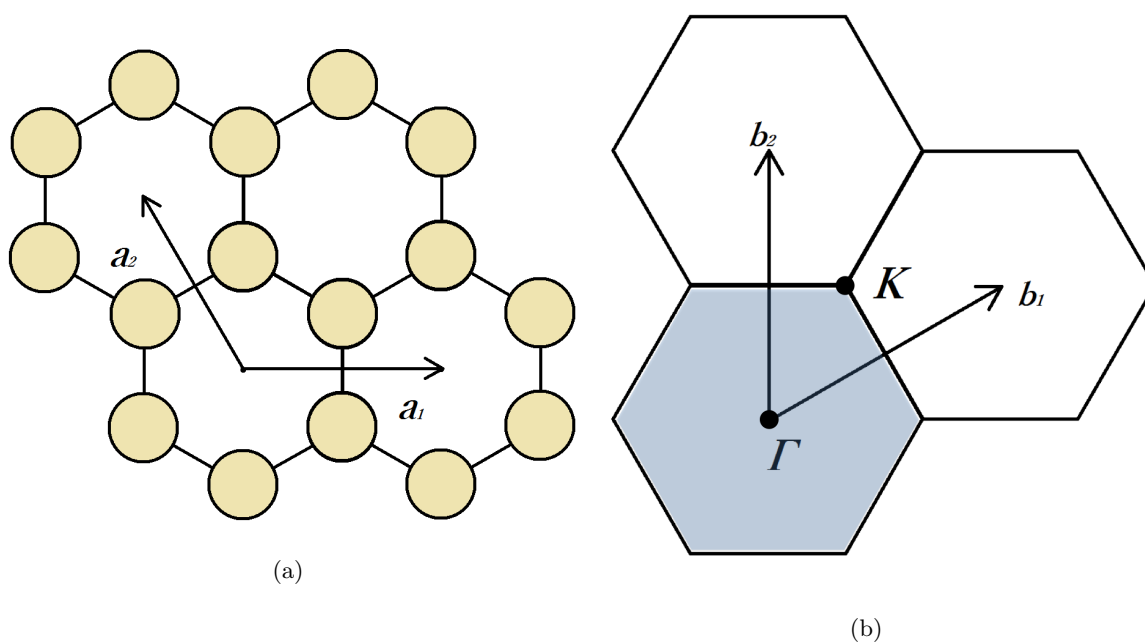
The lengths in the c-axis are 12Å and 30Å in the monolayer and bilayer graphene, respectively. The lattice constant is 2.46Å in the cases of the monolayer and bilayer graphene.

3.   Results And Discussion

3.1   Monolayer graphene

**Table I.**   Space group and point group of each k point in graphenes.

	monolayer graphene	bilayer graphene AA structure	bilayer graphene AB structure
space group	$P6/mmm$ $(191, D_{6h}^1)$	$P6/mmm$ $(191, D_{6h}^1)$	$P\bar{3}m1$ $(164, D_{3d}^3)$
Γ	D_{6h}	D_{6h}	D_{3d}
K	D_{3h}	D_{3h}	D_3
M	D_{2h}	D_{2h}	C_{2h}
T	C_{2v}	C_{2v}	C_2
T'	C_{2v}	C_{2v}	C_2
Σ	C_{2v}	C_{2v}	C_s

Fig. 1. Topview of monolayer graphene (a) and reciprocal space including the first Brillouin zone indicated by shaded area (b). a_1 and a_2 are the periodic lattice vectors and b_1 and b_2 are the primitive receiprocal lattice vectors.

We first study monolayer graphene whose periodic lattice vectors (a_1, a_2, a_3) and reciprocal lattice vectors (b_1, b_2, b_3) are defined in Fig.1. We show the band structure of monolayer graphene in Fig.2 and tabulate the high symmetry lines and points in Table.I. The Dirac cone appears at the K point, i.e., two linear bands are degenerated at the K point. The necessary condition for the emergence of the Dirac cone is that two wavefunctions are degenerated. Therefore, they must belong to the two-dimensional irreducible representation. Consequently, the point group at the Dirac point needs to include two-dimensional representation. In the present case, the symmetry of the K point is D_{3h} (Table.I), which includes two-dimensional irreducible representations (E' and E''). The Dirac cone point belongs to E''.

We tabulate the irreducible representations of the wavefunctions for the k point in Table.II. Our assignments of representations are somewhat different from those in Ref. 23 but are consistent with those in Ref. 24 (Some differences between our study and the past one (Ref. 24) in the assignment at the M point are found but they are expected to originate from the choice of the axes which are perpendicular to the principal axis). We take an example of the lowest energy level at the Γ point in Fig.2. The Γ point has the D_{6h} symmetry and our assignment for this level is A_{2u}, which is different from the
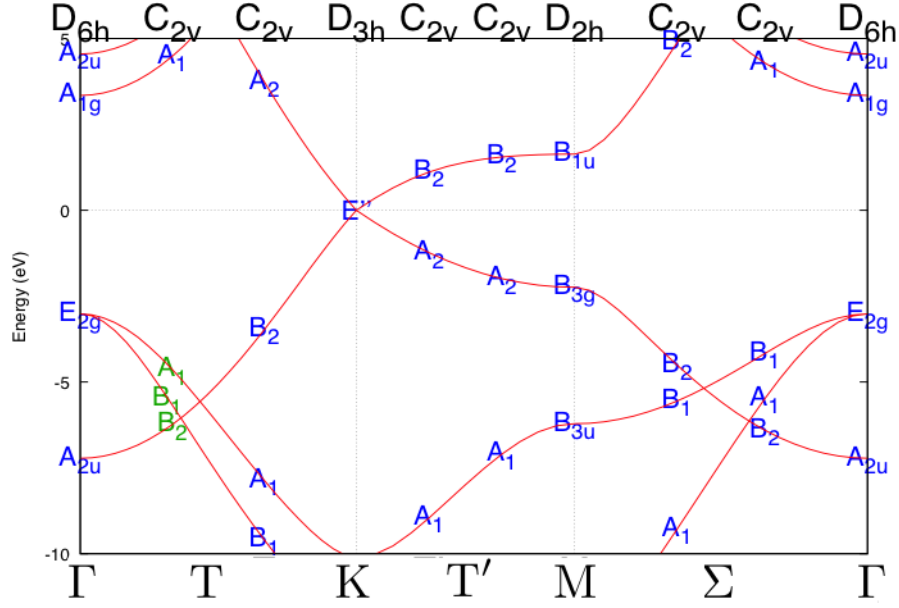
**Fig. 2.** Band structure of monolayer graphene. The energies are measured from the Fermi energy.

Table II. Representations of in monolayer graphene. We use the Mulliken notations[34] for the representation. The band index is in the descending energy order from the Fermi level.

k-points	band index	representation
Γ	1	E_{2g}
	2	A_{2u}
T	1	B_2
	2	A_1
	3	B_1
K	1	E''
	2	A'

assignment in Ref. 23 and is consistent with that in Ref. 24. It is clear from Fig.3 that the wavefunction has the characters of A_{2u} for all the symmetry operations in D_{6h}.

3.2 Bilayer graphenes

We perform LDA calculations and find that the layer distances are 3.37Å and 3.16 Å for the AA and AB stackings, respectively, and the energy in the AB stacking is 6.35×10^{-3}eV/atom lower than that of the AA stacking according to our calculation results. In the case of the AA stacking, the symmetry of the K point is D_{3h}, which is the same as that in the monolayer graphene. Among the six irreducible representations,

(a)   (b)
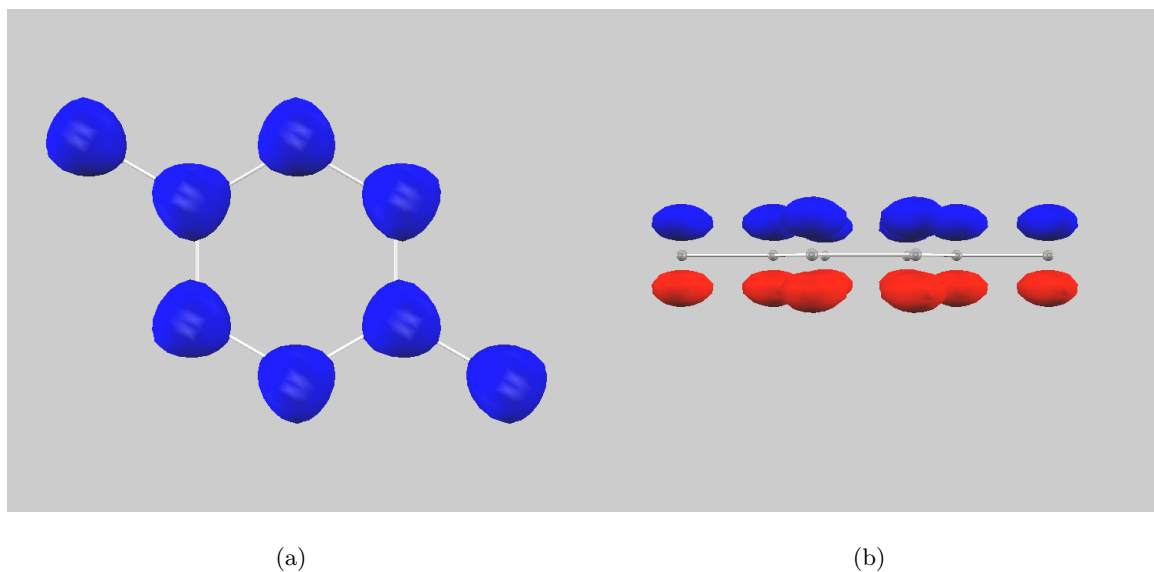
Fig. 3. Isosurface of wave functions of the lowest energy level at the Γ point in Fig.2. The vertical and horisontal views are showin in (a) and (b), respectively. The red and blue colors indicate plus and minus values.

there are two-dimensional irreducible representations (E' and E''). Near the Fermi level, two degenerated levels E' and E'' appear. On the other hand, in the case of the AB stacking, the symmetry of the K point is D_3, which is lower than that in the AA stacking. As a result, only one representation is two-dimensional (E), among the six representations in the D_3 symmetry. The degenerated level E appears at the Fermi level and two levels are located near the Fermi level. i.e., the A2 (A1) levels appear above (below) the Fermi level. The above-mentioned difference between the electronic structures near the Fermi energy is attributed to the high and low symmetries in the AA and AB stacking, respectively.

3.3 Monolayer silicene

We next study monolayer silicene. The two atoms in the unit cell are buckled as shown in Fig.5 and we tabulate the high symmetry lines and points in Table.III. In the optimized structure, the magnitude of the buckling is 0.41 Å according to the present calculation. Because of the buckling, the symmetry is D_{3d}, which is lower than D_{6h} of the non-buckled monolayer graphene. As a result, the symmetry of the K point is D_{3d}, which is lower than that of monolayer graphene (D_{3h}). The Dirac cone appears at the Fermi level and the representations are two-dimensional (E) as Fig.6 shows.

Overall the band structure of the silicene is similar to that of monolayer graphene. However, the some bands are crossing in the case of monolayer graphene whereas corre-
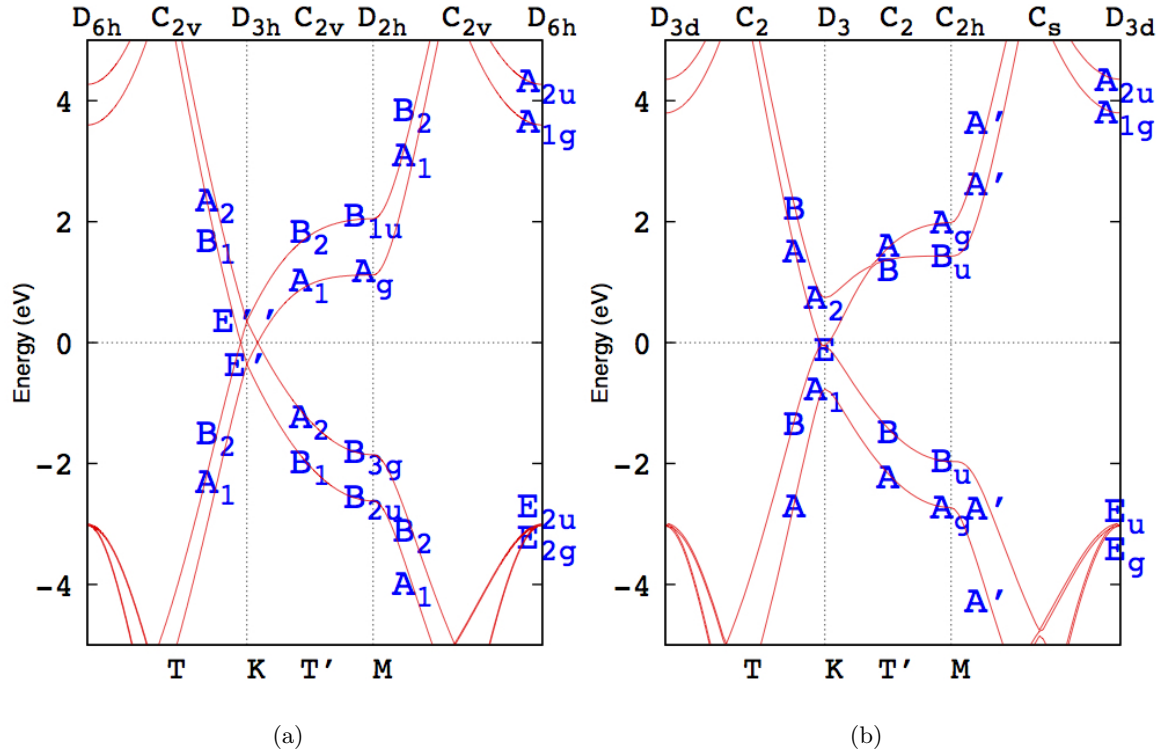
Fig. 4.   Band structures of bilayer graphenes whose stackings are AA (a) and AB (b).

Table III.   Space groups and the point groups of each k point in mono and bilayer silicenes.
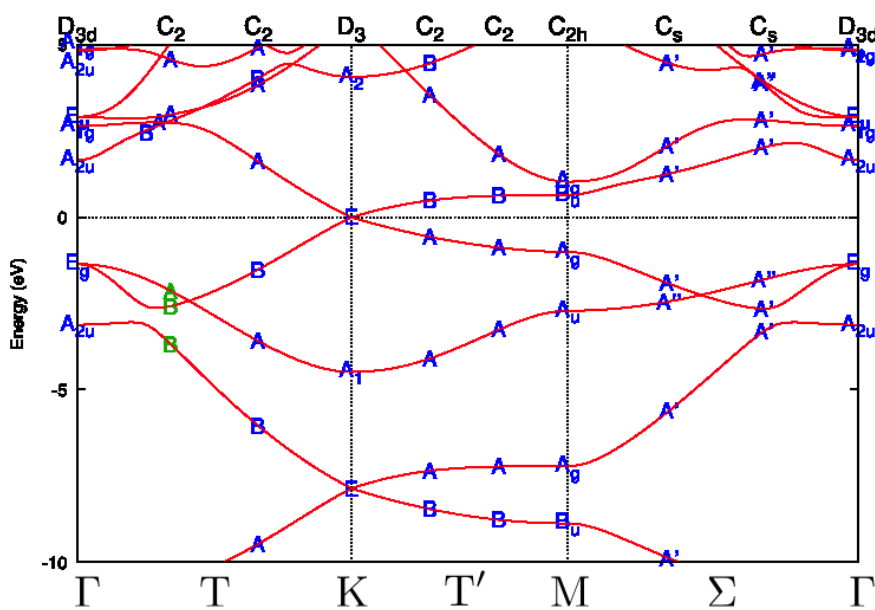
	monolayer silicene	bilayer silicene AA1 structure	bilayer silicene AA2 structure	bilayer silicene AB1 structure	bilayer silicene AB2 structure
space group	$P\bar{3}m1$ $(164,D_{3d}^3)$	$P\bar{3}m1$ $(164,D_{3d}^3)$	$P\bar{6}m2$ $(187,D_{3d}^1)$	$P\bar{3}m1$ $(164,D_{3d}^3)$	$P3m1$ $(156,C_{3v}^3)$
Γ	D_{3d}	D_{3d}	D_{3h}	D_{3d}	C_{3v}
K	D_3	D_3	C_{3h}	D_3	C_3
M	C_{2h}	C_{2h}	C_{2v}	C_{2h}	C_s
T	C_2	C_2	C_s	C_2	C_1
T'	C_2	C_2	C_s	C_2	C_1
Σ	C_s	C_s	C_{2v}	C_s	C_s

sponding bands are not crossed in the case of silicene. This non-crossing is due to that two bands belongs to the same representation because the symmetries are lower than those of monolayer graphene. For example, in the Γ-K line, the symmetry of silicene is C_2 (Fig.6) whereas the symmetry is C_{2v} in the case of monolayer graphene (Fig.2). The three bands (indicated by green characters in Fig.6) which near the Γ point and below the Fermi level belong to representations of A, B and B in the descending energy order from the Fermi level. On the other hand, the corresponding representations are A_1, B_1

(a)

(b)
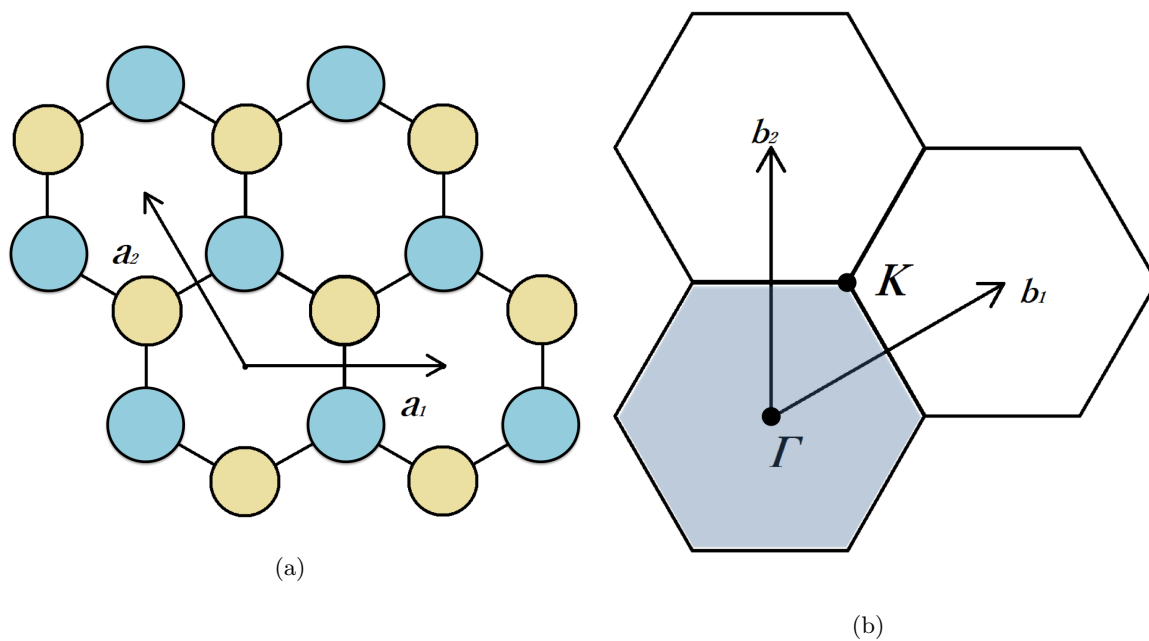
Fig. 5.   Atomic structure (a) and the reciprocal space (b) in silicene. The blue and yellow balls are not in the same plane in (a). The shaded area indicates the first-Brillouin zone in (b).

Fig. 6.   Band structure of monolayer silicene. The energies are measured from the Fermi level.

and B_2 in the case of monolayer graphene (Fig.2). Consequently, the second and third bands cross each other in the case of graphene whereas these two bands don't cross each other in the case of silicene (Fig.6).

3.4 Bilayer silicenes

AA1

(a)

AA2

(b)

AB1

(c)

AB2

(d)
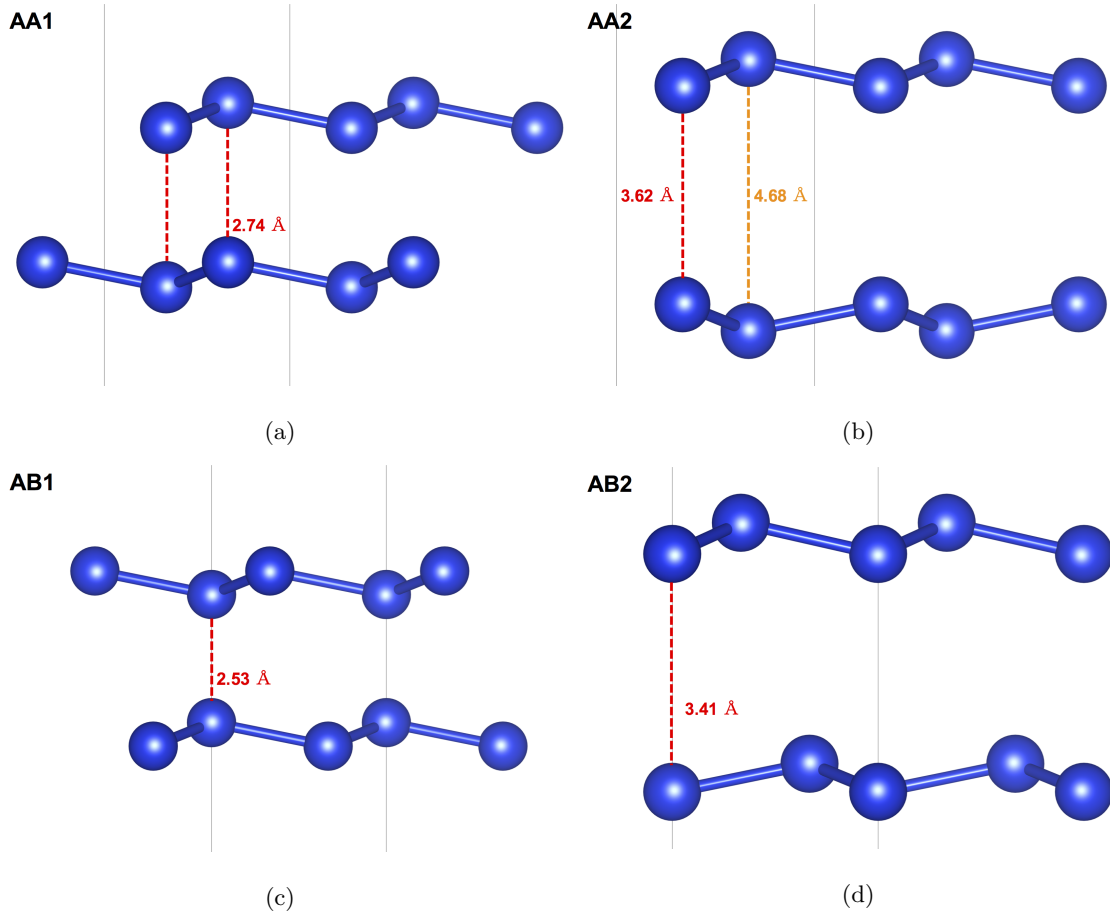
Fig. 7. Atomic structure of bilayer silicenes. They are distinguished by the stacking of atoms and the buckled structures of the layers and named AA1(a), AA2(b), AB1(c), AB2(d) structures.

Table IV. Total energies, the minimum atomic distances between the two layers, buckling distances and the minimum atomic distance between the two layers. Their total energies are measured from that of monolayer silicene.

	bilayer silicene AA1 structure	bilayer silicene AA2 structure	bilayer silicene AB1 structure	bilayer silicene AB2 structure
Total energy[eV/Atom]	-0.125	-0.0176	-0.142	-0.0309
The minimum atomic distance between the two layers [Å]	2.74	3.62	2.53	3.41
Buckling distance[Å]	0.81	0.53	0.65	0.51
Bond Length[Å]	2.38	2.30	2.33	2.29

We consider bilayer silicene. The minimum[35,36] and larger unit cells[37,38] were used in the past studies. It was recently reported that the most stable structure has a large

unit cell.[38)] However, we focus on the minimum cell since the main purpose of this paper is to clarify the condition that induces the Dirac cone.

We study the AA and AB stackings. We consider the two types of the AA stacking structures, i.e. AA1 and AA2. In the case of the AA1 (AA2) structure, the top and bottom layers have the same (inverted) buckling order (Fig.7). We also consider the two types of AB stacking structures. In the AB1 (AB2) structures, the top and bottom layers have the same (inverted) buckling order (Fig.7). We assume that the lattice constant of the bilayer is the same as that of the monolayer. We show the total energies and geometry parameters of their structures in Table.IV.

Table V. Character table of the K point in bilayer silicenes. $\varepsilon = e^{i\frac{2}{3}\pi}$.

			E	$C_3(z)$	$C_3^2(z)$	S_3	σ_h	S_3^5
C_3	E	e	1	ε	ε^*			
		e^*	1	ε^*	ε			
C_{3h}	E'	e'	1	ε	ε^*	ε^*	1	ε
		e'^*	1	ε^*	ε	ε	1	ε^*
	E''	e''	1	ε	ε^*	$-\varepsilon^*$	-1	$-\varepsilon$
		e''^*	1	ε^*	ε	$-\varepsilon$	-1	$-\varepsilon^*$

We show the band structures of bilayer silicenes in Fig.8. The AA1 and AB1 structures have the symmetry of D_{3d} at the Γ point. As a result, the symmetry of the K point of these strucutres is D_3. Since D_3 includes the two-dimensional representation E, some two bands cross each other at the K point. In particular, the Dirac cone at the Fermi level arises in the AB1 structure. On the other hand, the AA2 and AB2 structures have symmetries of C_{3h} and C_3, respectively. Since these symmetries are lower than D_3, the symmetries include no two-dimensional representation. It should be noticed that the Mulliken notations include representations of E' and E'' in the C_{3h} symmetry[34)] and these are not two-dimensional representation. Therefore, we use e and e^* insted of E because these (e and e^*) are one-dimensional representation (Table.V). As shown in Fig.8, there are no degenerate bands at the K point in the case of AA2 and AB2 structures.

(a)

(b)

(c)

(d)
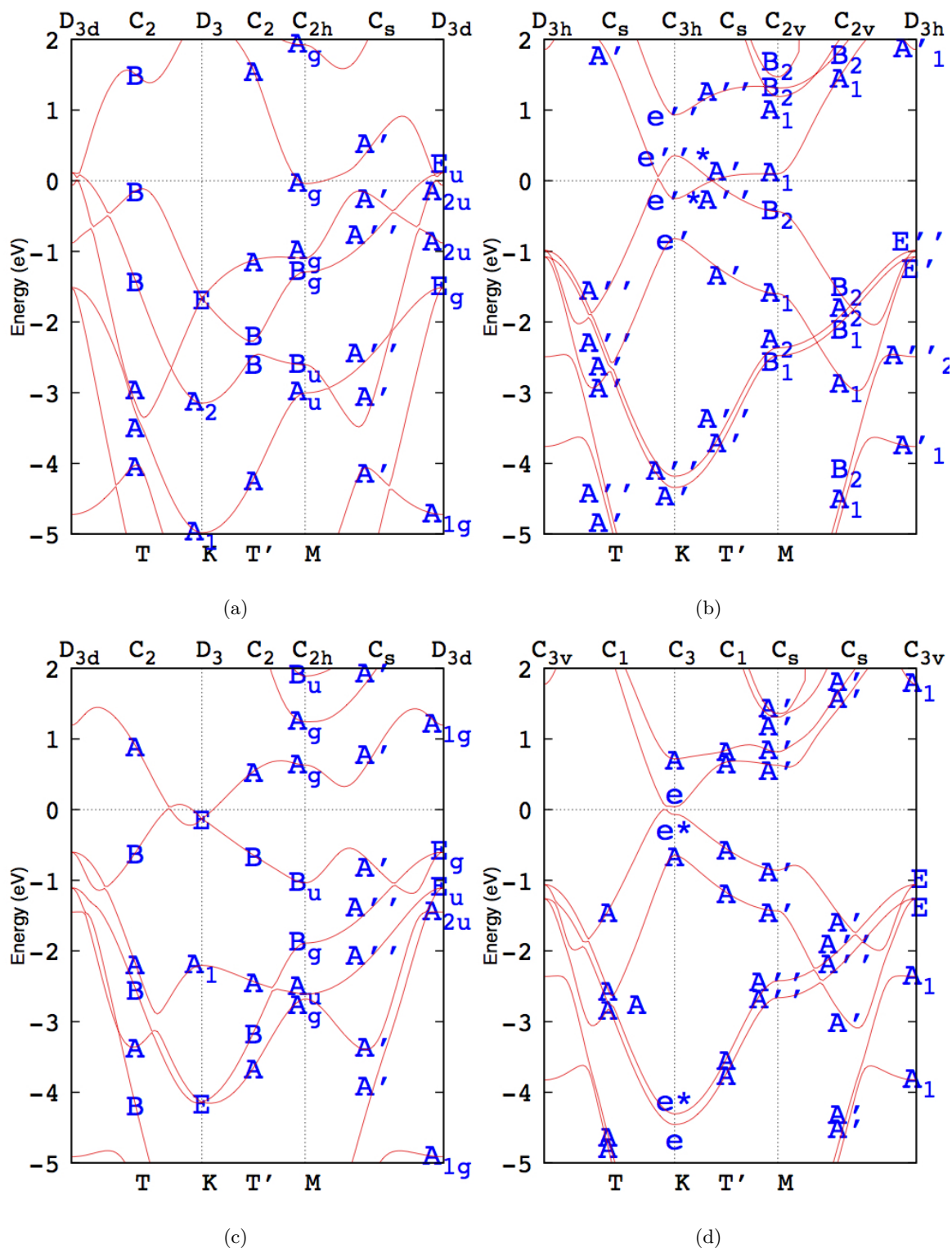
Fig. 8.   Band structures of bilayer silicenes forming (a)AA1, (b)AA2, (c)AB1 and (d)AB2 stacking structures.

3.5   Discussion

So far, we discussed the relation between appearance of Dirac cones and space symmetry. When symmetry is high enough to include two-dimensional representations, Dirac cones may appear and they do not appear when the symmetry does not include any two-dimensional representation.

The two-dimensional hexagonal systems have hexagonal and trigonal structures and the symmetries of them are C_{6h}, C_{3h}, C_{6v}, C_{3v}, C_6, C_3, S_6, D_{6h}, D_6, D_{3h}, D_{3d} and D_3. The symmetries at K point for these structures are C_{3v}, C_{3h}, C_3, D_{3h} and D_3. Among them, both C_{3h} and C_3 do not have two-dimensional representations though they include E-type representations in the Mulliken notation. Therefore Dirac cones are expected not to appear in the cases of C_{3h} and C_3.

4.   Conclusion

We carry out first-principles calculation of the structures of free-standing mono- and bi-layer graphenes and silicenes and analyze electronic structures based on the group theory. When the point group at the K point is high enough to include two-dimensional representations, the Dirac cone may appear and when the group does not include two-dimensional representations, the Dirac cone does not appear. Among the symmetries (C_{3v}, C_{3h}, C_3, D_{3h} and D_3) at the K point in the hexagonal and trigonal two-dimensional structures, C_{3h} and C_3 do not include two-dimensional representations and therefore Dirac cones do not appear.

Acknowledgment

References

1) A. K. Geim and K. S. Novoselov: Nat. Mater. **6** (2007) 183.

2) J. Wang, S. Deng, Z. Liu and Z. Liu: National Science Review **2** (1) (2015) 22.

3) A. H. Castro Neto, F. Guinea, N. M. R. Peres, K. S. Novoselov and A. K. Geim: Rev. Mod. Phys. **81** (2009) 109.

4) D. J. Appelhans, Z. Lin and M. T. Lusk: Phys. Rev. B **82** (2010) 073410.

5) L. M. Malard, M. H. D. Guimarães, D. L. Mafra, M. S. C. Mazzoni and A. Jorio: Phys. Rev. B **79** (2009) 125426.

6) J.-C. Charlier, J.-P. Michenaud and X. Gonze: Phys. Rev. B **46** (1992) 4531.

7) T. Ohta, A. Bostwick, T. Seyller, K. Horn and E. Rotenberg: Science **313** (2006) 5789.

8) S. A. Wolf, D. D. Awschalom, R. A. Buhrman, J. M. Daughton, S. von Molnár, M. L. Roukes, A. Y. Chtchelkanova and D. M. Treger: Science **294** (5546) (2001) 1488.

9) R. S. Edwards and K. S. Coleman: Nanoscale **5** (2013) 38.

10) L. P. Biro, P. Nemes-Incze and P. Lambin: Nanoscale **4** (2012) 1824.

11) L. Chen, C.-C. Liu, B. Feng, X. He, P. Cheng, Z. Ding, S. Meng, Y. Yao and K. Wu: Phys. Rev. Lett. **109** (2012) 056804.

12) P. Vogt, P. De Padova, C. Quaresima, J. Avila, E. Frantzeskakis, M. C. Asensio, A. Resta, B. Ealet and G. Le Lay: Phys. Rev. Lett. **108** (2012) 155501.

13) S. Huang, W. Kang and L. Yang: Appl. Phys. Lett. **102** (2013) 133106.

14) C.-L. Lin, R. Arafune, K. Kawahara, M. Kanno, N. Tsukahara, E. Minamitani, Y. Kim, M. Kawai and N. Takagi: Phys. Rev. Lett. **110** (2013) 076801.

15) E. Bianco, S. Butler, S. Jiang, O. D. Restrepo, W. Windl and J. E. Goldberger: ACS Nano **7** (5) (2013) 4414; PMID: 23506286.

16) F.-f. Zhu, W.-j. Chen, Y. Xu, C.-l. Gao, D.-d. Guan, C.-h. Liu, D. Qian, S.-C. Zhang and J.-f. Jia: Nat Mater **14** (10) (2015) 1020; Article.

17) H. Liu, A. T. Neal, Z. Zhu, Z. Luo, X. Xu, D. Tománek and P. D. Ye: ACS Nano **8** (4) (2014) 4033.

18) T. Hirahara, T. Nagao, I. Matsuda, G. Bihlmayer, E. V. Chulkov, Y. M. Koroteev, P. M. Echenique, M. Saito and S. Hasegawa: Phys. Rev. Lett. **97** (2006) 146803.

19) C. Herring: Phys. Rev. **52** (1937) 365.

20) X. Huang, Y. Lai, Z. Hang, H. Zheng and C. Chan: Nat Mater **10** (8) (2011) 582.

21) J. L. Mañes, F. Guinea and M. A. H. Vozmediano: Phys. Rev. B **75** (2007) 155424.

22) B. Bradlyn, J. Cano, Z. Wang, M. G. Vergniory, C. Felser, R. J. Cava and B. A. Bernevig: Science.

23) E. Kogan and V. U. Nazarov: Phys. Rev. B **85** (2012) 115418.

24) E. Kogan, V. U. Nazarov, V. M. Silkin and M. Kaveh: Phys. Rev. B **89** (2014) 165430.

25) V.Heine: *Group Theory in Quantum Mechanics* (Pergamon Press, 1960).

26) R. Knox and A. Gold: *Symmetry in the solid state* (W.A. Benjamin, 1964) Lecture notes and supplements in physics.

27) W. G. Harter: Journal of Mathematical Physics **10** (4) (1969) 739.

28) : https://azuma.nims.go.jp/cms1.

29) J. P. Perdew, K. Burke and M. Ernzerhof: Phys. Rev. Lett. **77** (1996) 3865.

30) J. P. Perdew and Y. Wang: Phys. Rev. B **45** (1992) 13244.

31) M. S. Alam, J. Lin and M. Saito: Japanese Journal of Applied Physics **50** (8R) (2011) 080213.

32) D. Vanderbilt: Phys. Rev. B **41** (1990) 7892.

33) D. R. Hamann, M. Schlüter and C. Chiang: Phys. Rev. Lett. **43** (1979) 1494.

34) R. S. Mulliken: J. Chem. Phys. **23** (1955) 1997.

35) M. Ezawa: J. Phys. Soc. Jpn. **81** (2012) 104713.

36) B. Mohan, A. Kumar and P. K. Ahluwalia: Physica E **53** (2013) 233.

37) J. E. Padilha and R. B. Pontes: The Journal of Physical Chemistry C **119** (7) (2015) 3818.

38) Y. Sakai and A. Oshiyama: Phys. Rev. B **91** (2015) 201405.